

# Nucleation and early growth of anodized TiO<sub>2</sub> film

A. Jaroenworarluck<sup>a)</sup>

*MTEC: National Metal and Materials Technology Center, Klong Luang,  
Pathumthani 12120, Thailand*

D. Regonini, C.R. Bowen, and R. Stevens

*Materials Research Centre, Department of Mechanical Engineering, University of Bath,  
Claverton Down BA2 7AY, United Kingdom*

(Received 2 October 2007; accepted 21 March 2008)

Anodized films of titanium were prepared under different controlled conditions in a water-based electrolyte containing fluorine ions, using either a constant potential or a potential gradually rising to 20 V. The films were then examined using transmission electron microscopy at different stages of growth, in particular, the very early stages of growth (30 s, 200 s, and 10 min) and when the ordered nano-tubular structure was finally established (2–4 h). The use of ramped voltage during the early stages of anodization allowed a well-interconnected porous network to develop and maintained active oxidation throughout anodization. The film, as formed, consisted mainly of amorphous oxide/hydroxides of titanium with small regions of nano-sized crystals. These were found more often in the denser regions of the amorphous network, particularly the arms of the coral-like structure that formed. As the anodized film grew in thickness, the pores tended to become aligned, leading to a surface layer of nanotubes on the electrode material. Electron optical characterization revealed that the nanotubes consist of a stack of rings where the passage of the current had been optimized.

## I. INTRODUCTION

Titanium oxide is an important material largely used as a white pigment in paints and food as well as ultra-violet (UV) ray protection in cosmetic products. It is of great interest to scientists and technologists for its chemical and physical properties and its stability.<sup>1</sup> It is suitable for many applications including biomedical,<sup>2–7</sup> gas-sensors,<sup>8–14</sup> photo-catalysis,<sup>15–23</sup> protection of light-sensitive materials,<sup>24</sup> and solar cell devices.<sup>25–32</sup> In all these technologies, a very high surface area, in the form of nano-sized particles or nanotubes is required to maximize efficiencies and performance. Anodization, sol-gel, hydrothermal, and vapor deposition are some of the techniques normally used to generate different morphologies of the nanostructured titanium dioxide.<sup>33,34</sup>

### A. Anodization

The generation of titania nanotubes via anodization of metallic titanium is a relatively new topic.<sup>35,36</sup> Generally, a small addition of fluorine ions is required to initiate the

formation of cavities in the anodic structure, enhancing conductivity and creating channels where current can flow,<sup>37</sup> although aqueous electrolytes containing chloride ions have also been used.<sup>38,39</sup> The tubes have been shown to consist of a remnant structure formed as a result of the collapse of the oxide/hydroxide gel formed by the electrochemical oxidation. This structure is made of interlocked rings produced by the collapse of the cavities formed in the gel layer. The passage of a current through the gel as a flux, normal to the metallic titanium electrode and the electrolyte, causes the cavities to line up, and when breakthrough occurs, to form a tubular structure.<sup>40</sup> The electronic/ionic conductivity of the gel layer and its viscosity clearly play a significant role in the formation of such tubes.

Recently, long tubular structures have been produced using organic electrolytes, therefore minimizing the amount of water in the electrolytic solution. For example, 7- $\mu\text{m}$ -thick tubes can be generated in a glycol-based electrolyte, which has a considerably lower electrical conductivity but a much higher viscosity.<sup>41</sup> Tubes up to 320  $\mu\text{m}$  long have been grown by Grimes and coworkers using polar organic electrolytes to enhance the extraction of Ti<sup>4+</sup> from the metal and inhibiting the growth of the barrier layer at the metal/oxide interface by using larger cations in the salts for a source of fluorine ions.<sup>42–45</sup>

<sup>a)</sup>Address all correspondence to this author.

e-mail: angkhanj@mtec.or.th  
DOI: 10.1557/JMR.2008.0276

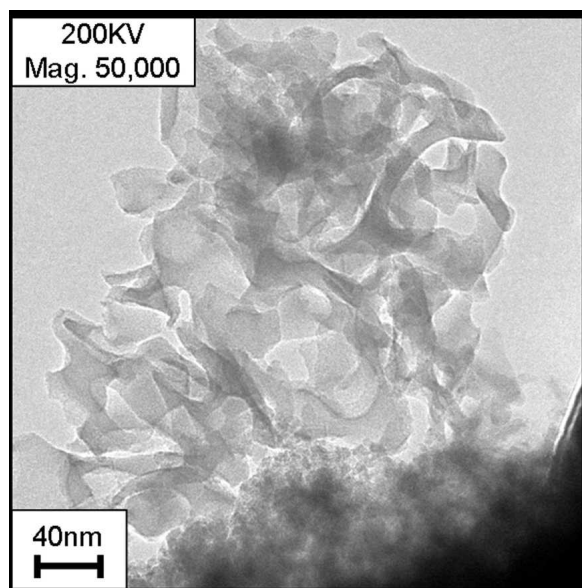


FIG. 1. Specimen anodized for 30 s with a voltage ramp (100 mV/s); the experiment was stopped at 3 V. As can be observed, pores and cavities have already formed.

Nanotubes up to 1000  $\mu\text{m}$  have also been grown using ethylene-glycol-based electrolytes.<sup>46</sup> Schmuki et al. have obtained similar results<sup>47</sup> and enhanced the self-organization of the nanotube array by using a multistep anodization process.<sup>48</sup> It is of interest to note that tubes formed using organic electrolytes with a small water content (<0.5 wt%) are smooth, while those formed in water-based media or organic media with a high water content have a rougher outer surface with ridges apparent on the tube walls.<sup>49</sup>

## B. Nanotube formation mechanism

Several mechanisms for the formation of titania nanotubes have been proposed, involving the growth of pits into scallop-shaped pores, which lead to the generation of nanotubes, the initial development of a disordered “wormlike” structure, or a pH gradient between the top and the bottom of the pores.<sup>28,37,50–53</sup> Previous transmission electron microscopy (TEM) observations by the authors,<sup>40,54</sup> 30 min into the anodization process, revealed that a series of interconnected cavities are initially developed, which allow current to flow within the oxide/hydroxide film. Published mechanisms to date have not predicted such an interconnected structure, since they infer that a series of pits are initially formed through the barrier layer oxide.

## C. Aims

The aim of this work was to examine the anodized titania film at different stages, in particular the very early stages of growth (30 s, 200 s, and 10 min). The samples

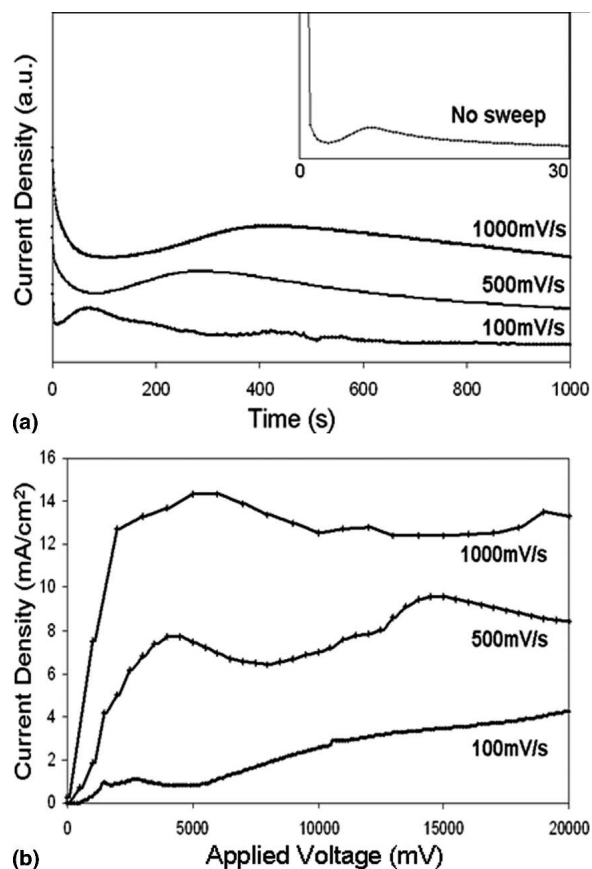


FIG. 2. (a) Current-time registered during the anodization of Ti samples after applying different sweep rates to the final constant voltage (20 V) and (b) I-V curves registered during the voltage ramp stage.

used in the present work have not undergone ion beam thinning, since previous TEM<sup>40</sup> revealed that ion beam thinning can cause sufficient heating to crystallize regions of the thin film. While Mor et al. used a voltage ramp, rather than constant voltage, to produce tapered nanotubes,<sup>50</sup> we also observed that thicker tubes are obtained by applying an initial voltage ramp (or “sweep”).<sup>54</sup> Here, our approach consisted of application of a voltage sweep at the beginning of anodization and using TEM to study its effect on the development of the oxide and the tubular/porous network. Characterizing the very early stages of growth during the voltage ramp (30 s), at the end of a voltage ramp (200 s), and after the voltage ramp (10 min to 4 h) will elucidate the growth mechanism.

## II. EXPERIMENTAL METHODS

A commercially pure (99.6%) titanium sheet (0.5 mm thick) was used as a substrate. Before being electrochemically oxidized, the titanium was ultrasonically cleaned in an isopropyl alcohol bath. Anodizing was performed by applying a variety of sweep rates (100, 500, and 1000 mV/s) to reach the final value of 20 V, and the

potential was then held at 20 V for different times (10 min to 4 h). In the context of this work, the term “sweep rate” (or “ramp”) defines the rate at which the voltage increases upward toward 20 V. In experiments for the 100 mV/s sweep rate, the process was interrupted before (after 30 s) or at the end of the sweep to 20 V (after 200 s) to investigate the early stages of the process by TEM. For comparison, one of the samples was anodized at constant voltage (20 V) without application of a voltage ramp. Using a Teflon electrochemical cell, the metal surface was exposed to the electrolyte (1 M Na<sub>2</sub>SO<sub>4</sub> + 0.5 wt% of NaF) at the anode, while a platinum mesh was used as a counter electrode (cathode). The electrolyte temperature was held constant at 20 °C. The anodized specimens were examined by scanning electron microscopy (SEM) and TEM (models JEOL JEM2010 and JEOL JEM 1200, Japan). TEM samples were prepared by detaching portions of the oxide film from the substrate, mounting them in a double layer 200 mesh copper grid, and observing them directly at 120 or 200 kV.

### III. RESULTS AND DISCUSSION

The decision to characterize the early stages of the growth process (30 s, 200 s, and 10 min) predominantly by TEM was made because SEM can view only the upper surface features of the developing oxide.

#### A. Structure at 30 s

A TEM image of a sample anodized for 30 s with a sweep rate of 100 mV/s (i.e., experiment stopped at 3 V) is shown in Fig. 1. There is a barrier-type (pore free) layer, which can represent either the thermal oxide layer naturally formed on the metal once exposed to air or simply a portion of the oxide anodically formed at the metal/oxide interface, which has yet to be etched by fluorine ions. Figure 1 shows that the nucleation of pores and cavities has already started, as shown by the interconnected network above the barrier layer. Considering the high level of interconnection registered in the anodic layer (at least at the beginning of the process), it is unlikely to have a pH gradient between different parts of the

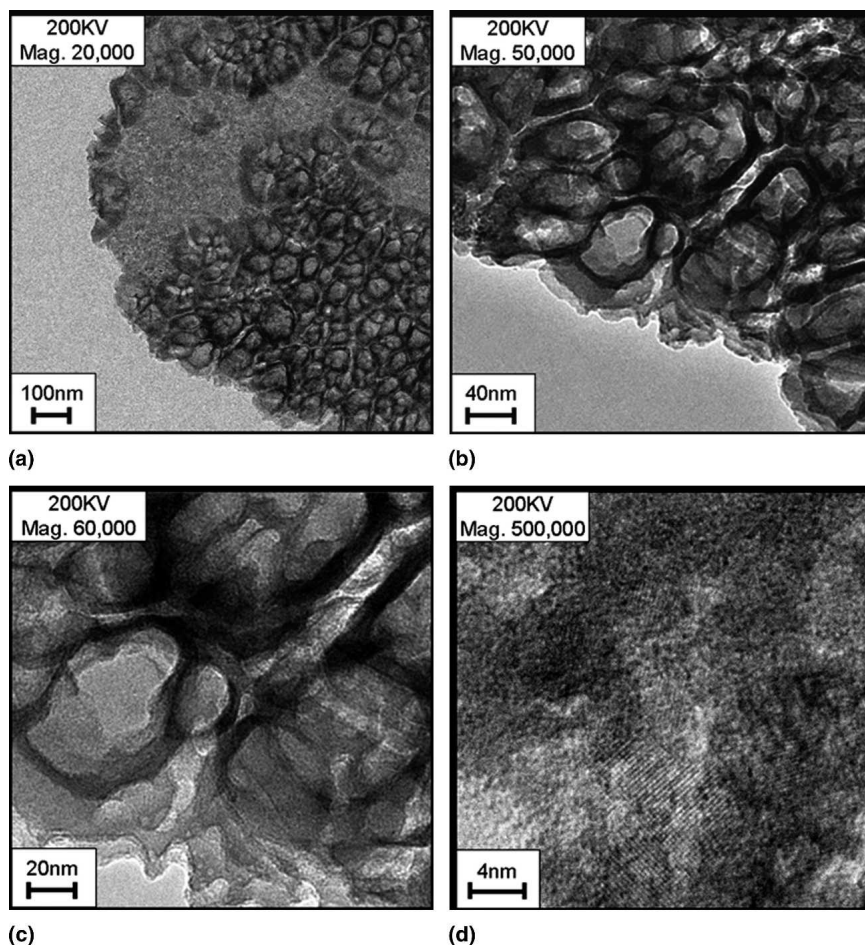
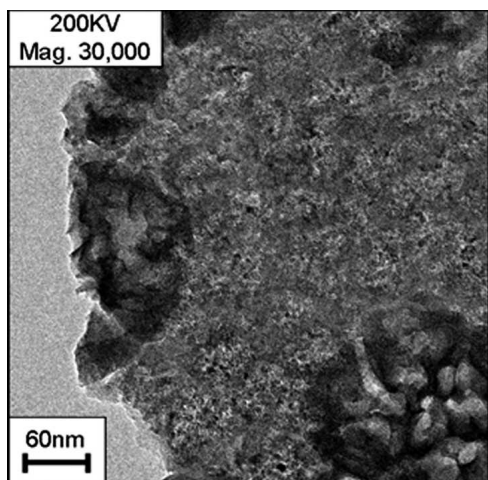
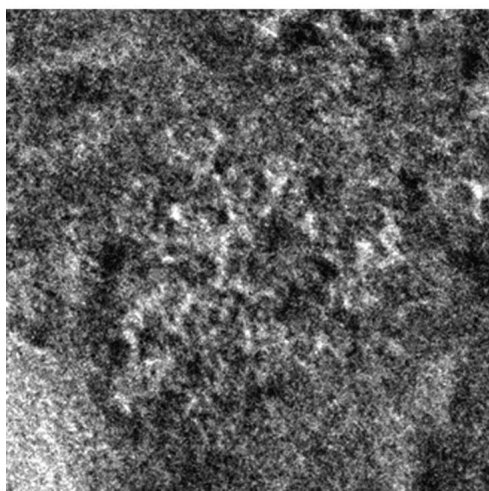


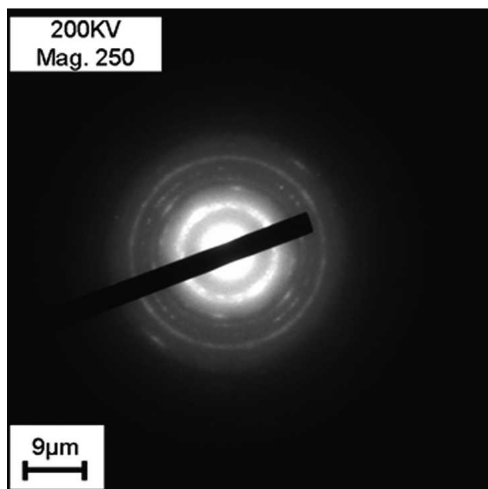
FIG. 3. (a) TEM micrographs of the layer adjacent to the thermally oxidized film, (b) higher magnification images showing the 3D network of anodized TiO<sub>2</sub> making up the structure, and (c) lattice image showing the amorphous nature of the anodic layer, but (d) also the presence of very small region of crystalline material. This sample was anodized for 200 s; the experiment stopped at the end of the sweep rate of 100 mV/s (20 V).



(a)

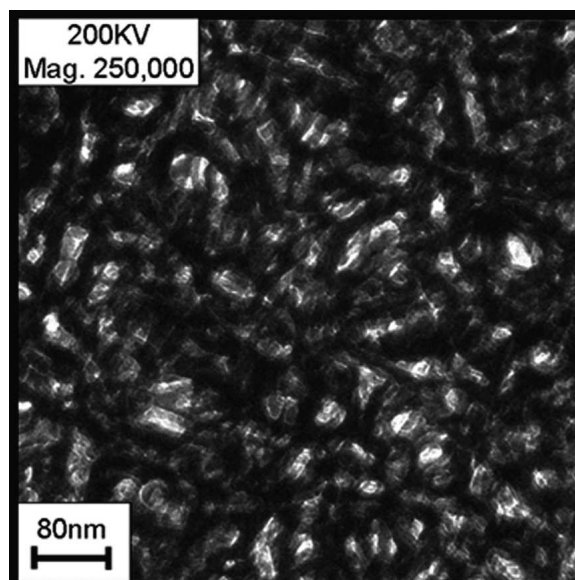


(b)

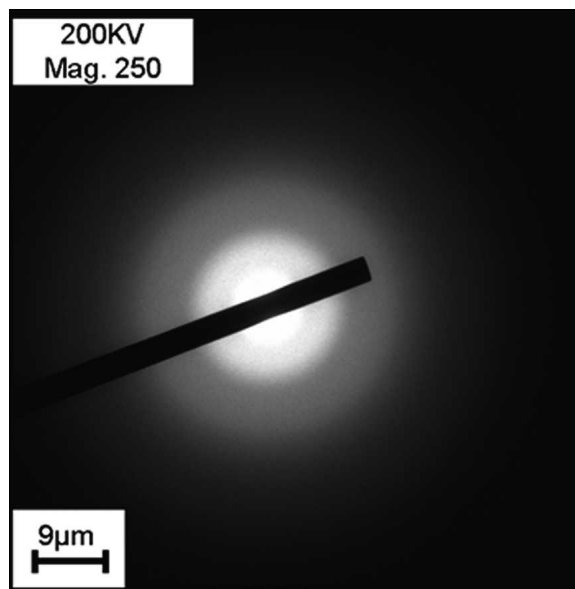


(c)

FIG. 4. TEM images of a sample anodized for 200 s: (a) low-magnification image of the forming porous layer, (b) high-magnification image of the same area suggesting the presence of small islands of crystalline phase within the arms of the structure, and (c) diffraction pattern confirming the presence of crystals.



(a)

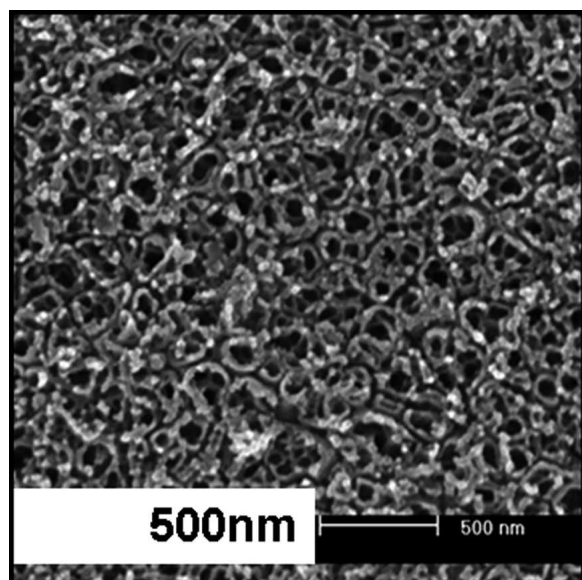


(b)

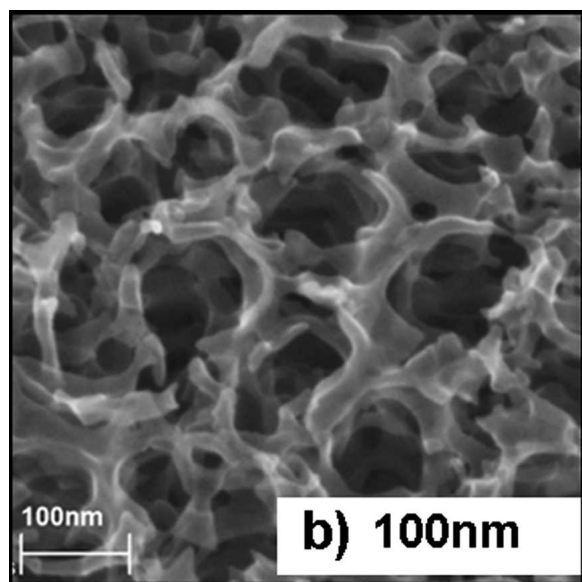
FIG. 5. TEM images of a specimen anodized for 10 min: (a) the oxide consists of a porous network in which the cavities appear random, and (b) the diffraction pattern suggests the anodic outer layer is amorphous.

film, as previously reported.<sup>53</sup> Since the specimen is anodized for 30 s, it is reasonable to assume that the development of cavities starts almost simultaneously with the formation of the oxide. In contrast to previous work under potentiostatic conditions, a barrier layer (approximately 50 nm at 25 V) is immediately formed before any etching by fluorine ions commences.<sup>37</sup>

The inset of Fig. 2(a) shows the current transient registered when a constant voltage (20 V) is applied without any initial ramp. The current drops to a minimum value quickly since the barrier layer at the metal/oxide (M/MO)



(a)



(b)

FIG. 6. SEM images of a specimen anodized for 2 h. (a) The tubular-like morphology is clearly visible at low magnification, and the structure appeared more defined than the one obtained after 10 min. (b) At higher magnification, oxide rings forming the tubes can be clearly seen beneath the top layer.

interface reaches its maximum thickness within seconds. The current then rises as a result of pore formation and finally becomes constant. For any given electrolyte and voltage, the rate of electrochemical oxidation is mainly determined by the thickness of this barrier layer beneath the porous structure.<sup>42–45</sup> So the oxidation process remains active, ions are required to move through this insulating layer by ionic conduction. Finally, the current becomes constant, indicating equilibrium between the competing electrochemical oxidation and chemical dis-

solution. Although ionic conduction through the porous layer is higher than that in the underlying barrier layer, electrochemical oxidation at the oxide/electrolyte interface will decrease as the depth of the nanotubes increases. Near equilibrium, the ratio between electrochemical oxidation and chemical dissolution changes slowly until the oxidation and dissolution rates at the mouth of each nanotube (oxide/electrolyte interface) are equal and nanotube thickness is no longer time dependent.

A somewhat different scenario develops if the same voltage (20 V) is applied after an initial voltage ramp. Figure 2(a) shows the current transient registered after application of different sweep rates (mV/s) to reach the final voltage, 20 V. The current decays to a minimum, indicating that the barrier layer at the M/MO interface has achieved its maximum thickness, and then rises when pores are generated in the freshly formed hydroxide layer and links with cavities already formed during the voltage ramp. The current then becomes almost constant or decreases slowly, suggesting an approach to equilibrium conditions. This results in a constant thickness layer of nanotubes regardless of anodization time. The conditions used here allow growth of 1.5–2- $\mu\text{m}$ -thick nanotube layers, twice the thickness achieved under the same conditions (voltage, electrolyte, time), but with no initial sweep,<sup>40</sup> confirming that in the latter case the barrier layer quickly reaches its maximum thickness. The use of a voltage ramp allows pore nucleation to occur on a relatively thin metal oxide film, thus optimizing the current flow through the insulating oxide layer. Chemical dissolution is determined mainly by fluorine concentration and solution pH and is constant. However, with a voltage ramp, the growth rate of the oxide starts from a minimum and progressively increases with the increase in voltage. This allows the development of cavities and pores before the structure corresponding to the final voltage, 20 V, is formed and stabilized. Current passing through this porous network of channels contributes to postponing the point at which electrochemical etching balances the chemical dissolution.

It is interesting to note that at higher sweep rates (e.g., 1000 mV/s), the equilibrium point is postponed to longer times [Fig. 2(a)]. This could well be related to the reduced diffusion layer developed at the higher sweep rate, which more readily allow fluorine ions to etch the surface. Figure 2(b) shows current–voltage curves registered from samples anodized at different sweep rates. During the upward ramp, it can be seen that current rises and then becomes almost constant. The resistance of the oxide increases with thickness, but this is overcome by the increasing voltage and by the nucleation and development of linked cavities. This has been clearly shown in the TEM micrographs (Fig. 1) to take place from the very early stages (30 s) of the anodizing process.

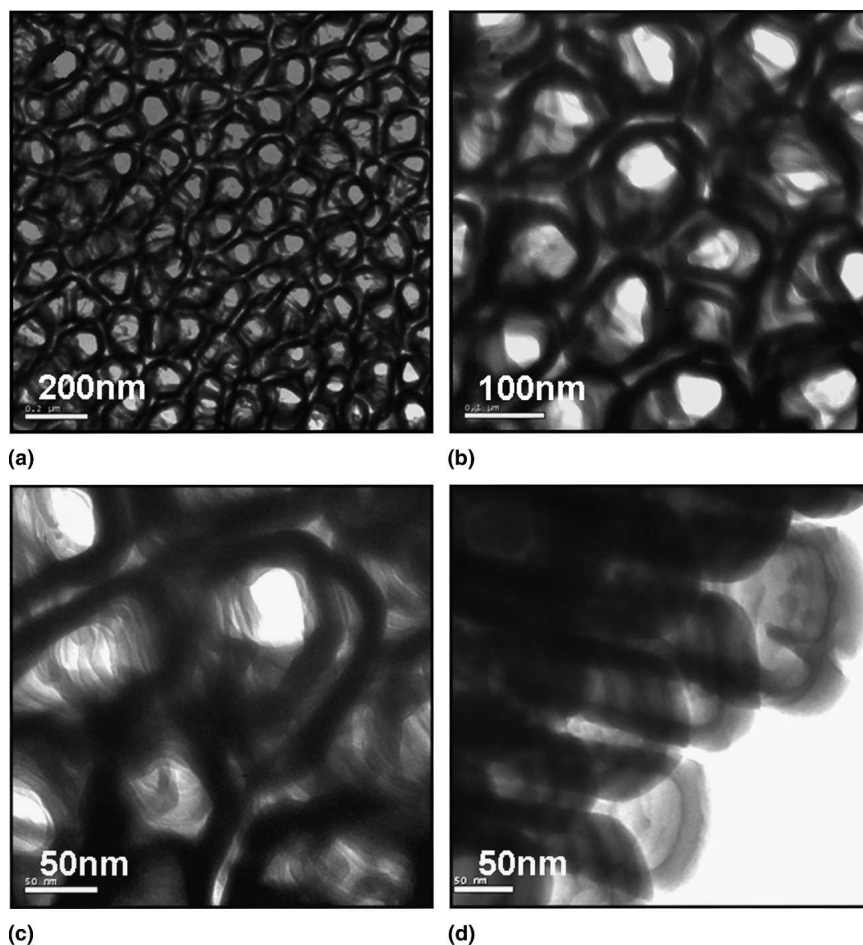


FIG. 7. (a–c) The specimen was anodized for 4 h and has a regular porous network, while (d) a cross-sectional image taken by tilting the sample reveals the presence of different rings, which are piled together to form a nanotube-like structure.

## B. Structure at 200 s

Figures 3(a)–3(c) offer further information of the anodic oxide, once the voltage ramp is terminated at 20 V (200 s at 100 mV/s). The sample was prepared from the anodized layer lifted off the surface of the electrode and dispersed on a carbon film supported on a 200 mesh copper grid. The film consists of an arrangement of dense arms around a central low-density cavity or pore, the specimen being transparent to the electron beam. At the edge of the specimen where the film has fractured, the morphology of the arms of the structure is more apparent, and they can be seen to form a three-dimensional (3D) network surrounding the cavities. The micrograph in Fig. 3(a) shows a fine-grained structure made up of two regions, the first being the fine-grained interface layer and the second the anodized oxide on which has developed the network of arms of the 3D mesh. It is clear in Figs. 3(b) and 3(c) that the network formation at this stage is dependent on the formation of cavities, which vary in shape and, to a degree, in size. Indeed, within one of the cavities, several smaller cavities can be seen which stabilize the structure. It is also apparent that many of the

cavities have linked up and that a passage exists through the anodized TiO<sub>2</sub> film, which will allow the movement of Ti<sup>4+</sup> ions between the anode surface and the electrolyte and therefore the controlled growth of the film. Figure 3(d) shows distinct regions of amorphous material together with very small (~8–10 nm) regions of crystalline material, evident from the lattice imaging.

Oxide growth<sup>55</sup> has been reported to proceed via titanium hydroxyl intermediates that are later dehydrated to the oxides. The anodized layer, seen in Fig. 4(a), consists of a remnant skeleton, possibly that of a hydroxide gel that initially forms and subsequently dehydrates. The series of channels grow via the linking of pores, which leads to the development of the arrays of nanotubes on the surface of the titanium electrode. The structure at first sight appears to be amorphous and will appear so under x-ray diffraction (XRD) examination as a consequence of the small crystallite size. Close inspection at very high TEM magnifications [Fig. 4(b)] gives some indication of occasional crystallinity in that there are small islands of crystalline phase ~1–2 nm diameter within the arms of the structure. Such a structure indicates that the gel is on

the point of crystallization and the nuclei present have been formed by the random differences in concentration, temperature, or anode interface morphology. The presence of very fine crystals is also indicated by the continuous rings [Fig. 4(c)]. The presence of larger crystals with small ones could be responsible for the generation of the elongated spots. Zhao et al.<sup>52</sup> revealed that nanotubes were partially crystalline at 20V/30 min and that the crystallization was thought to be related to dielectric breakdown. Clearly, crystalline regions are present at very early stages of growth (200 s).

### C. Structure at 10 min

After a somewhat longer anodizing treatment (10 min), a thicker layer of the porous TiO<sub>2</sub> phase is formed, which is still transparent to the electron beam [Fig. 5(a)]. This allowed the electron diffraction pattern [Fig. 5(b)] to be taken, which clearly shows this outer film is amorphous with no sign of crystallinity. The structure of the amorphous film is at this stage developing into a partially ordered arrangement of connected pores having a rough interior surface. The shapes of the “tubes” are still highly irregular, not yet having equilibrated under the driving forces, such as surface tension, active within the film.

### D. Structure at 2–4 h

The minimum anodization time required to obtain a relatively organized nanotube structure is 90–120 min. After 2 h, the self-order of the structure has increased compared to 10 min, as can be seen in Figs. 6 and 7. The tubular-like morphology is clearly visible using SEM at low magnification [Fig. 6(a)]. At higher magnification [Fig. 6(b)], the oxide rings pile up to create the nanotubes and can be clearly observed beneath the top layer. Additional details are provided by TEM images, as shown in Figs. 7(a)–7(d). Figure 7(d), taken from a tilted sample (45°) shows a cross-sectional view of the tubes and again confirms that the anodic layer prepared in a water-based electrolyte is better described as formed from a stack of rings rather than smooth tubes.<sup>40</sup>

An aspect rarely mentioned in previous growth models is the evolution of oxygen at the anode, which occurs during anodization of titanium.<sup>56</sup> For all our experiments, gas evolution was observed at the anode, particularly during the early stages of the process. The initial porous structure is formed in the presence of fluorine but is possibly aided by water electrolysis at the anode. In addition, the presence of channels where electrolyte and ions can flow also enables continued oxygen evolution, while for barrier-layer (pore-free) type TiO<sub>2</sub>, oxygen evolution occurs only at the very early stages of growth.

## IV. CONCLUSIONS

The use of a ramped voltage during the early stages of anodization allows a well-interconnected porous network

to form and maintains oxidation for a longer period. TEM analysis has provided new insight into the development of nanotube growth. Within a very short time (30 s), the structure of the film becomes porous and remains amorphous (up to 200 kV electrons) in nature. However, there is some evidence of small, isolated regions of ordered structure in the as-prepared anodized film at 200 s. The crystallites tend to form in the more dense arms of the coral-like structure that develops as the pores start to link up to form tubular structures. The morphology of the structure arises when the anodized film is in an amorphous state. This facilitates rearrangement of the nanostructure of the film under the influence of the electrical potential across it during the anodization process by enhancing ionic conduction of the active species particularly at free surfaces, where rapid ion transfer by means of the liquid electrolyte could take place. As the anodized film increases in thickness, the pores link up and form a kinked tubular structure through the thickness of the film (10 min), eventually straightening after an extended time (>2 h) and becoming aligned perpendicular to the electrode surface, leading to the formation of a stack of rings. Any mechanistic model of titania nanotube formation must be able to account for the development and growth of such a series of structures.

## ACKNOWLEDGMENTS

This work is a part of the project supported financially by National Metal and Materials Technology Center (MTEC) under project fund No. MT-B-48-CER-07-190-I. The Department of Microelectronics of the Slovak University of Technology and International Laser Center (Bratislava) is also acknowledged for providing SEM.

## REFERENCES

1. U. Diebold: The surface science of titanium dioxide. *Surf. Sci. Rep.* **48**, 53 (2003).
2. X. Zhu, K.H. Kim, and Y. Jeong: Anodic oxide films containing Ca and P of titanium biomaterial. *Biomaterials* **22**, 2199 (2001).
3. B.C. Yang, M. Uchida, H.M. Kim, X.D. Zhang, and T. Kokubo: Preparation of bioactive titanium metal via anodic oxidation treatment. *Biomaterials* **25**, 1003 (2004).
4. S.H. Oh, R.R. Finönes, C. Daraio, L.H. Cen, and S. Jin: Growth of nano-scale hydroxyapatite using chemically treated titanium oxide nanotubes. *Biomaterials* **26**, 4938 (2005).
5. T. Kokubo, T. Matsushita, and H. Takadama: Titania-based bioactive materials. *J. Eur. Ceram. Soc.* **27**, 1553 (2007).
6. K.C. Popat, L. Leoni, C.A. Grimes, and T.A. Desai: Influence of engineered titania nanotubular surfaces on bone cells. *Biomaterials* **28**, 3188 (2007).
7. K.C. Popata, M. Eltgroth, T.J. LaTempad, C.A. Grimes, and T.A. Desai: Decreased staphylococcus epidermis adhesion and increased osteoblast functionality on antibiotic-loaded titania nanotubes. *Biomaterials* **28**, 4880 (2007).
8. K. Zakrzewska: Gas sensing mechanism of TiO<sub>2</sub>-based thin films. *Vac.* **74**, 335 (2004).

9. S. Akbar, P. Dutta, and C. Lee: High-temperature ceramic gas sensors: A review. *Int. J. Appl. Ceram. Technol.* **3**, 302 (2006).
10. G.K. Mor, M.A. Carvalho, M.V. Pishko, and C.A. Grimes: A room-temperature TiO<sub>2</sub>-nanotube hydrogen sensor able to self-clean photoactively from environmental contamination. *J. Mater. Res.* **19**, 628 (2004).
11. O.K. Varghese and C.A. Grimes: Metal oxide nanoarchitectures for environmental sensing. *J. Nanosci. Nanotech.* **3**, 277 (2003).
12. O.K. Varghese, D. Gong, M. Paulose, K.G. Ong, and C.A. Grimes: Hydrogen sensing using titania nanotubes. *Sens. Actuators, B* **93**, 338 (2003).
13. O.K. Varghese, D. Gong, M. Paulose, K.G. Ong, E.C. Dickey, and C.A. Grimes: Extreme changes in the electrical resistance of titania nanotubes with hydrogen exposure. *Adv. Mater.* **15**, 624 (2003).
14. M. Paulose, O.K. Varghese, G.K. Mor, C.A. Grimes, and K.G. Ong: Unprecedented ultra-high hydrogen gas sensitivity in undoped titania nanotubes. *Nanotechnology* **17**, 398 (2006).
15. M.A. Fox and M.T. Dulay: Heterogeneous photocatalysis. *Chem. Rev.* **93**, 341 (1993).
16. M.R. Hoffmann, S.T. Martin, W. Choi, and D.W. Bahnemann: Environmental applications of semiconductor photocatalysis. *Chem. Rev.* **95**, 69 (1995).
17. A. Mills, G. Hill, S. Bhopal, I.P. Parkin, and S.A. O'Neill: Thick titanium dioxide films for semiconductor photocatalysis. *J. Photochem. Photobiol., A* **160**, 185 (2003).
18. G.K. Mor, K. Shankar, O.K. Varghese, and C.A. Grimes: Photoelectrochemical properties of titania nanotubes. *J. Mater. Res.* **19**, 2989 (2004).
19. B.M. Reddy, I. Ganesh, and A. Khan: Stabilization of nanosized titania-anatase for high temperature catalytic applications. *J. Mol. Catal. A: Chem.* **223**, 295 (2004).
20. H.D. Jang, S-K. Kim, and S-J. Kim: Effect of particle size and phase composition of titanium dioxide nanoparticles on the photocatalytic properties. *J. Nanopart. Res.* **3**, 141 (2001).
21. T. Minabe, D.A. Tryk, P. Sawunyama, Y. Kikuchi, K. Hashimoto, and A. Fujishima: TiO<sub>2</sub>-mediated photodegradation of liquid and solid organic compounds. *J. Photochem. Photobiol., A* **137**, 53 (2000).
22. G.K. Mor, K. Shankar, M. Paulose, O.K. Varghese, and C.A. Grimes: Enhanced photocleavage of water using titania nanotube arrays. *Nano Lett.* **5**, 191 (2005).
23. A. Fujishima, T.N. Rao, and D.A. Tryk: Titanium dioxide photocatalysis. *J. Photochem. Photobiol., C* **1**, 1 (2000).
24. M. Zayat, P.G. Parejo, and D. Levy: Preventing UV-light damage of light sensitive materials using a highly protective UV-absorbing coating. *Chem. Soc. Rev.* **36**, 1270 (2007).
25. M. Grätzel: Photoelectrochemical cells. *Nature* **414**, 338 (2001).
26. M. Grätzel: Review: Dye-sensitized solar cells. *J. Photochem. Photobiol., C* **4**, 145 (2003).
27. C. Longo and M.A. De Paoli: Dye-sensitized solar cells: A successful combination of materials. *J. Braz. Chem. Soc.* **14**, 889 (2003).
28. G.K. Mor, O.K. Varghese, M. Paulose, K. Shankar, and C.A. Grimes: A review on highly ordered, vertically oriented TiO<sub>2</sub> nanotube arrays: Fabrication, material properties, and solar energy applications. *Sol. Energy Mater. Sol. Cells* **90**, 2011 (2006).
29. J.H. Park, S. Kim, and A.J. Bard: Novel carbon-doped TiO<sub>2</sub> nanotube arrays with high aspect ratios for efficient solar water splitting. *Nano Lett.* **6**, 24 (2006).
30. J.M. Macák, H. Tsuchiya, A. Ghicov, and P. Schmuki: Dye-sensitized anodic TiO<sub>2</sub> nanotubes. *Electrochem. Commun.* **7**, 1133 (2005).
31. G.K. Mor, K. Shankar, M. Paulose, O.K. Varghese, and C.A. Grimes: Use of highly-ordered TiO<sub>2</sub> nanotube arrays in dye-sensitized solar cells. *Nano Lett.* **6**, 215 (2006).
32. N-G. Park, J. Van de Lagemaat, and A.J. Frank: Comparison of dye-sensitized rutile-and anatase-based TiO<sub>2</sub> solar cells. *J. Phys. Chem. B* **104**, 8989 (2000).
33. X. Chen and S.S. Mao: Synthesis of titanium dioxide (TiO<sub>2</sub>) nanomaterials. *J. Nanosci. Nanotech.* **6**, 906 (2006).
34. D.V. Bavykin, J.M. Friedrich, and F.C. Walsh: Protonated titanates and TiO<sub>2</sub> nanostructured materials: Synthesis, properties, and applications. *Adv. Mater.* **18**, 2807 (2006).
35. V. Zwillling, E. Darque-Ceretti, A. Boutry-Forveille, D. David, M.Y. Perrin, and M. Aucouturier: Structure and physicochemistry of anodic oxide films on titanium and TA6V alloy. *Surf. Interface Anal.* **27**, 629 (1999).
36. D. Gong, C.A. Grimes, O.K. Varghese, W. Hu, R.S. Singh, Z. Chen, and E.C. Dickey: Titanium oxide nanotube arrays prepared by anodic oxidation. *J. Mater. Res.* **16**, 3331 (2001).
37. L.V. Taveira, J.M. Macák, H. Tsuchiya, L.F.P. Dick, and P. Schmuki: Initiation and growth of self-organized TiO<sub>2</sub> nanotubes anodically formed in NH<sub>4</sub>F/(NH<sub>4</sub>)<sub>2</sub>SO<sub>4</sub> electrolytes. *J. Electrochem. Soc.* **152**, B405 (2005).
38. R. Hahn, J.M. Macak, and P. Schmuki: Rapid anodic growth of TiO<sub>2</sub> and WO<sub>3</sub> nanotubes in fluoride free electrolytes. *Electrochem. Comm.* **9**, 947 (2007).
39. N.K. Allam and C.A. Grimes: Formation of vertically oriented TiO<sub>2</sub> nanotube arrays using a fluoride free HCl aqueous electrolyte. *J. Phys. Chem. C* **111**, 13028 (2007).
40. A. Jaroenworoluck, D. Regonini, C.R. Bowen, R. Stevens, and D. Allsopp: Macro, micro and nanostructure of TiO<sub>2</sub> anodized films prepared in a fluorine-containing electrolyte. *J. Mater. Sci.* **42**, 6729 (2007).
41. J.M. Macak, H. Tsuchiya, L. Taveira, S. Aldabergerova, P. Schmuki: Smooth anodic TiO<sub>2</sub> Nanotubes. *Angew. Chem. Int. Ed. Engl.* **44**, 7463 (2005).
42. M. Paulose, K. Shankar, S. Yoriya, H.E. Prakasham, O.K. Varghese, G.K. Mor, T.A. Latempa, A. Fitzgerald, and C.A. Grimes: Anodic growth of highly ordered TiO<sub>2</sub> nanotube arrays to 134 μm in length. *J. Phys. Chem. B* **110**, 16179 (2006).
43. K. Shankar, G.K. Mor, A. Fitzgerald, and C.A. Grimes: Cation effect on the electrochemical formation of very high aspect ratio TiO<sub>2</sub> nanotube arrays in formamide-water mixtures. *J. Phys. Chem. C* **111**, 21 (2007).
44. H.E. Prakasham, K. Shankar, M. Paulose, O.K. Varghese, and C.A. Grimes: A new benchmark for TiO<sub>2</sub> nanotube array growth by anodization. *J. Phys. Chem. C* **111**, 7235 (2007).
45. C.A. Grimes: Synthesis and application of highly ordered arrays of TiO<sub>2</sub> nanotubes. *J. Mater. Chem.* **17**, 1451 (2007).
46. M. Paulose, H.E. Prakasham, O.K. Varghese, L. Peng, K.C. Papat, G.K. Mor, T.A. Desai, and C.A. Grimes: TiO<sub>2</sub> nanotube arrays of 1000 μm length by anodization of titanium foil: Phenol red diffusion. *J. Phys. Chem. C* **111**, 14992 (2007).
47. S.P. Albu, A. Ghicov, J.M. Macak, and P. Schmuki: 250 μm long anodic TiO<sub>2</sub> nanotubes with hexagonal self-ordering. *Phys. Status Solidi (RRL)* **1**, 65 (2007).
48. J.M. Macak, S.P. Albu, and P. Schmuki: Towards ideal hexagonal self-ordering of TiO<sub>2</sub> nanotubes. *Phys. Status Solidi (RRL)* **1**, 181 (2007).
49. K.S. Raja, T. Gandhi, and M. Misra: Effect of water content of ethylene glycol as electrolyte for synthesis of ordered titania nanotubes. *Electrochem. Comm.* **9**, 1069 (2007).
50. G.K. Mor, O.K. Varghese, M. Paulose, N. Mukherjee, and C.A. Grimes: Fabrication of tapered, conical-shaped titania nanotubes. *J. Mater. Res.* **18**, 2588 (2003).
51. K. Yasuda, J.M. Macak, S. Berger, A. Ghicov, and P. Schmuki:

- Mechanistic aspects of the self-organization process for oxide nanotube formation on valve metals. *J. Electrochem. Soc.* **154**, C472 (2007).
52. J. Zhao, X. Wang, R. Chen, and L. Li: Fabrication of titanium oxide nanotube arrays by anodic oxidation. *Solid State Commun.* **134**, 705 (2005).
53. J.M. Macak, H. Tsuchiya, and P. Schmuki: High-aspect-ratio TiO<sub>2</sub> nanotubes by anodisation of titanium. *Angew. Chem. Int. Ed. Engl.* **44**, 2100 (2005).
54. D. Regonini, C.R. Bowen, R. Stevens, D. Allsopp, and A. Jaroenworoluck: Anodised TiO<sub>2</sub> nano-tubes: Voltage ramp influence on the nano-structured oxide and investigation of phase changes promoted by thermal treatments. *Phys. Status Solidi A* **204**, 1814 (2007).
55. Y.Z. Huang and D.J. Blackwood: Characterisation of titanium oxide film grown in 0.9% NaCl at different sweep rates. *Electrochim. Acta* **51**, 1099 (2005).
56. Y. Sul, C.B. Johansson, Y. Jeong, and T. Albrektsson: The electrochemical oxide growth behaviour on titanium in acid and alkaline electrolytes. *Med. Eng. Phys.* **23**, 329 (2001).